

Hinode Observations of the Onset Stage of a Solar Filament Eruption*

Alphonse C. STERLING,^{1,2} Ronald L. MOORE,¹ Thomas E. BERGER,³ Monica BOBRA,⁴ John M. DAVIS,¹
Patricia JIBBEN,⁴ Ryohei KANO,⁵ Loraine L. LUNDQUIST,⁴ D. MYERS,⁶ Noriyuki NARUKAGE,² Taro SAKAO,²
Kiyoto SHIBASAKI,⁷ Richard A. SHINE,³ Theodore D. TARBELL,³ and Mark WEBER⁴

¹NASA/Marshall Space Flight Center, VP62/Space Science Office, Huntsville, AL 35805, USA
asterling@spd.aas.org

²Institute of Space and Astronautical Science, Japan Aerospace Exploration Agency,
3-1-1 Yoshinodai, Sagamihara, Kanagawa 229-8510

³Lockheed Palo Alto Research Laboratory, Bldg 252, 3251 Hanover Street, Palo Alto, CA 94304, USA

⁴Harvard-Smithsonian Center for Astrophysics, 60 Garden Street, MS-58, Cambridge MA 02138, USA

⁵National Astronomical Observatory of Japan, 2-21-1 Osawa, Mitaka, Tokyo 181-8588

⁶Adnet Systems, Inc., 164 Rollins Avenue, Suite 303, Rockville, MD 20852, USA

⁷Nobeyama Radio Observatory, Minamimaki, Minamisakun, Nagano 384-1305

(Received 2007 June 30; accepted 2007 September 11)

Abstract

We used Hinode X-Ray Telescope (XRT) and Solar Optical Telescope (SOT) filtergraph (FG) Stokes-V magnetogram observations, to study the early onset of a solar eruption that includes an erupting filament that we observe in TRACE EUV images. The filament undergoes a slow rise for at least 20 min prior to its fast eruption and strong soft X-ray (SXR) flaring; such slow rises have been previously reported, and the new Hinode data elucidate the physical processes occurring during this period. XRT images show that during the slow-rise phase, an SXR sigmoid forms from apparent reconnection low in the sheared core field traced by the filament, and there is a low-level intensity peak in both EUV and SXRs during the slow rise. MDI and SOT FG Stokes-V magnetograms show that the pre-eruption filament is along a neutral line between opposing-polarity enhanced network cells, and the SOT magnetograms show that these opposing fields are flowing together and canceling for at least six hours prior to eruption. From the MDI data we measured the canceling network fields to be ~ 40 G, and we estimated that $\sim 10^{19}$ Mx of flux canceled during the five hours prior to eruption; this is only $\sim 5\%$ of the total flux spanned by the eruption and flare, but apparently its tether-cutting cancellation was enough to destabilize the sigmoid field holding the filament and resulted in that field's eruption.

Key words: Sun: filaments — Sun: flares — Sun: UV radiation — Sun: X-rays, gamma rays

1. Introduction

One of the major unsolved issues of solar physics is the cause of the onset of solar eruptions. These eruptions involve magnetic regions on the Sun of various size scales, and lead to solar flares and coronal mass ejections (CMEs). In recent years the importance of CMEs in particular has become better appreciated, as their role in space weather and its affects on the Earth have become more clear. Such concerns have deepened our desire to understand the cause of solar eruptions, and eventually how to predict them. The Hinode satellite, launched in 2006 September, contains an array of powerful solar instruments that will help us better understand solar eruptions and their cause. Here we present an example of a solar eruption observed by Hinode on 2007 March 2. We used the Hinode data in combination with those from the TRACE and SOHO missions to study the processes leading up to this eruption.

Eruptions involving filaments are instructive, since the filament can act as a tracer of the otherwise-invisible coronal

field, and in particular motions of the filament just prior to eruption indicate how the field evolves when it is on the verge of exploding. Sometime prior to eruption the filament typically shows activity intimating possible impending eruption (Roy & Tang 1975; Rust 1976), and the filament also often begins a relatively slow rise (“slow-rise phase”) prior to eruption (e.g., Tandberg-Hanssen et al. 1980; Kahler et al. 1988; Feynman & Ruzmaikin 2004). For quiet region events, the pre-eruption slow-rise phase can last several hours (Sterling & Moore 2004, Sterling et al. 2007) but it can be much shorter, ~ 10 min, for active-region eruptions (Sterling & Moore 2005; Williams et al. 2005). The 2007 March 2 event occurred in an active region, and accordingly the pre-eruption evolution was relatively quick. Hinode and TRACE, however, have sufficient time and spatial resolution to follow the pre-eruption dynamics. Here we present observations of the filament from TRACE, and the soft X-ray (SXR) and detailed magnetic field evolution from Hinode. As the Hinode magnetic data available for this event are not yet calibrated, we also used co-temporal, but spatially and temporally more coarse magnetic field data from the Michelson Doppler Imager (MDI) magnetograph on the SOHO spacecraft.

* Movies for figures 1, 2, and 4 are available in the electronic version (<http://pasj.asj.or.jp/v59/sp3/59s337/>).

2. Instrumentation and Data

Overall, the eruption itself was rather weak in SXR, peaking at a GOES class B2.5 level on 2007 March 2 at 05:29 UT, with the GOES data showing substantial enhancements from about 05:02 UT, and the event was located at about $300''$ west of disk center near the equator. The filament that erupts is visible in absorption in the EUV images from TRACE. At least portions of it are disturbed from the time of our earliest TRACE images at 04:28 UT, and it undergoes a slow rise prior to erupting, as discussed below (subsection 3.3).

The Hinode satellite (Kosugi et al. 2007) contains three instruments: the Solar Optical Telescope, SOT (Tsuneta et al. 2007), the X-Ray Telescope, XRT (Golub et al. 2007), and the EUV Imaging Spectrometer, EIS (Culhane et al. 2007); here we used data from the first two of these.

From SOT we used magnetograms constructed from the SOT filtergraph (FG) set to the magnetically-sensitive 6302 Å line. SOT was observing the Stokes-I and Stokes-V components in this line, and we used the Stokes-V data, which represent the line-of-sight magnetic field. Each original frame is 2048×1024 pixels, with a pixel size of $0''.16$. We used 21 frames between 22:20 UT on March 1 and 04:54 UT on March 2, with images nominally every 7 min, but with a gap between 22:55 UT and 03:16 UT, when data were not available.

From XRT we used images taken with its “Ti-poly” and “thick Al” filters, both of which have broad temperature response functions with peak temperature responses of several MK. Response at lower temperatures, however, is different, with Ti-poly sensitive to plasmas cooler than 1 MK, while the thick Al becomes substantially responsive to plasmas of about 2 MK and hotter. Our basic data set consists of 48 512×512 -pixel images between 04:01 UT and 05:47 UT on March 2, with a typical cadence of 2 min and a pixel size of $1''.032$. This time period began before the primary pre-eruption SXR emissions started, and continued past the time of peak flare intensity.

We have EUV data of the eruption from TRACE (Handy et al. 1998), specifically from its 171 Å filter, which has a peak response at about 1 MK. We used images from the start of the TRACE observations of this region on March 2 at 04:28 UT, until 06:27 UT, with a typical cadence of 1 min and a pixel size of $0''.5$. We also used full-disk magnetograms from MDI (Scherrer et al. 1995), which have $2''$ pixels; for the time of this event these images were taken only once about every 5 hours. Despite their lower cadence and lower spatial resolution compared to SOT, we used these MDI magnetograms because they are calibrated, while the SOT magnetograms have yet to be calibrated. In addition, the field of view of the SOT magnetogram is restricted and does not cover the entire filament, while we can select out subimages from MDI that cover the whole region of interest.

We aligned the various data sets as follows. Since the instrument pointing parameters are well understood for TRACE and SOHO, we can overlay TRACE EUV images onto MDI magnetograms accurately. We can align the SOT magnetograms with the MDI magnetograms by comparing frames from similar times. We then initially aligned XRT

images onto SOT magnetograms, and subsequently onto MDI magnetograms, using preliminary alignment information among the three Hinode instruments derived within the Hinode team (H. Hara 2007, private correspondence; N. Narukage 2007, private correspondence). We then adjusted the alignment by eye, e.g., matching bright features in the XRT images with stronger magnetic elements. Based on the matching of such features across the field of view that we used, we estimated our final alignment to be accurate to $< 10''$.

3. Observations and Analysis

Movies 1, 2, and 3 respectively are constructed from the TRACE, XRT, and SOT FG Stokes-V images.

3.1. EUV Evolution

Figure 1 shows TRACE frames of the erupting region, with an MDI magnetogram overlaid (see also movie 1). Prior to eruption the filament is activated and moves upward, with the filament obviously having changed position between figures 1a and 1b (see subsection 3.3). A new EUV loop (red arrow in figure 2b) brightens from its westernmost-side base beginning at 04:37 UT, and the illumination propagates along the loop, reaching the apex at about 04:42 UT and the opposite (east) base at about 04:51 UT. Over the first 5 minutes we estimate that this brightening travels about 50000 km from the west base to the apex, giving a velocity of $\sim 170 \text{ km s}^{-1}$, to about a factor of two. In figure 1c the filament is starting violent motions coinciding with the onset of flare brightenings.

3.2. SXR Evolution

Figure 2 shows images from XRT overlaid onto the same MDI magnetogram as that in figure 1, and panels (a), (b), and (d) of figure 2 roughly correspond respectively to panels (a), (b), and (c) of figure 1. Figure 2a is prior to the start of the obvious pre-eruption brightenings. Figure 2b, about 20 min prior to the main flare, shows a sigmoid loop developing. From movies made from these XRT images (movie 2), this loop appears to be developing near the locations indicated by the white and black arrows in the figure. This loop begins with what appears as an outflow from this location between images at 04:28 UT and 04:30 UT, and by the next image at 04:32 UT the entire northern “elbow” of the sigmoid (Moore et al. 2001) is discernible. By 04:45 UT it is a detached sigmoid loop, with the north elbow indicated by the red arrow in figure 2b. This sigmoid loop continues to expand outward, and appears to arch out to a more semicircular shape by the time of figures 2d and 2e, although much of this erupting sigmoid is obscured by saturation in the XRT images. From this time the arched sigmoid structure is escaping from the Sun as the field apparently opens up, and is beyond the frame’s field of view in figure 2f. On average, between images at 05:12 UT and 05:21 UT the outward-moving front (red arrows in figures 2d and 2e) has velocity of about 100 km s^{-1} , in the plane normal to the line-of-sight. This could, however, correspond to the accelerating structure seen in SXR by Alexander, Metcalf, and Nitta (2002). At earlier times it appears that similar but fainter sigmoid loops were ejected from the same location, suggesting formation by sequential

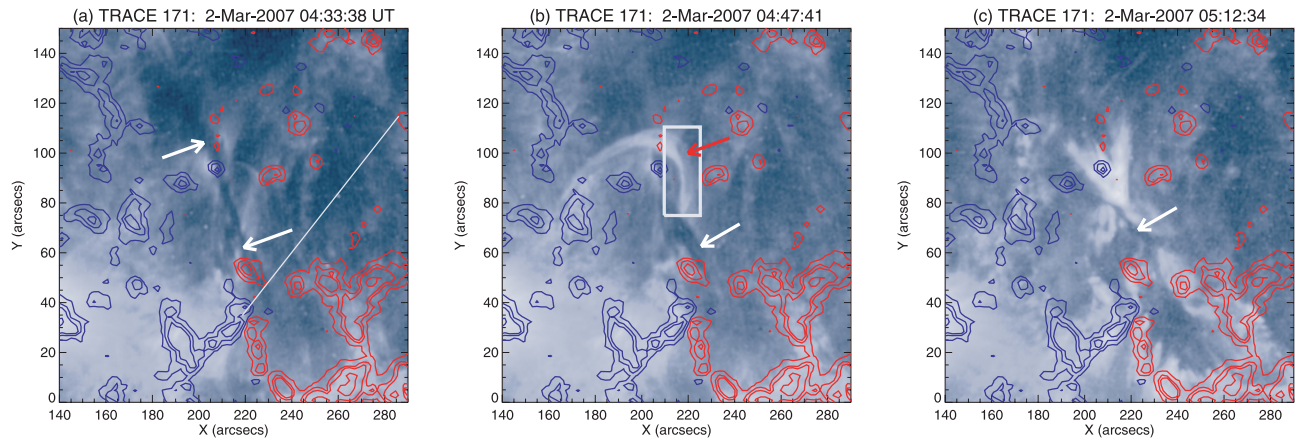


Fig. 1. TRACE 171Å images of the erupting filament (white arrows), and a new loop that brightened during the pre-eruption phase (red arrow in b). Red and blue contours are respectively positive and negative polarities from an MDI magnetogram from 04:51 UT on 2007 March 2; contour levels are 15, 50, 100, and 300 G. Panels (a) and (b) span a pre-eruption phase when the filament is undergoing a slow rise and other motions, and panel (c) is from near the time of onset of the filament's fast eruption. In (a) the white fiducial line is used to determine the filament height as a function of time in figure 3, and the box in (b) is for generating the lightcurve of figure 3. North is up and east to the left in these and all images in this paper. Movie 1 is provided for TRACE images as on-line material.*

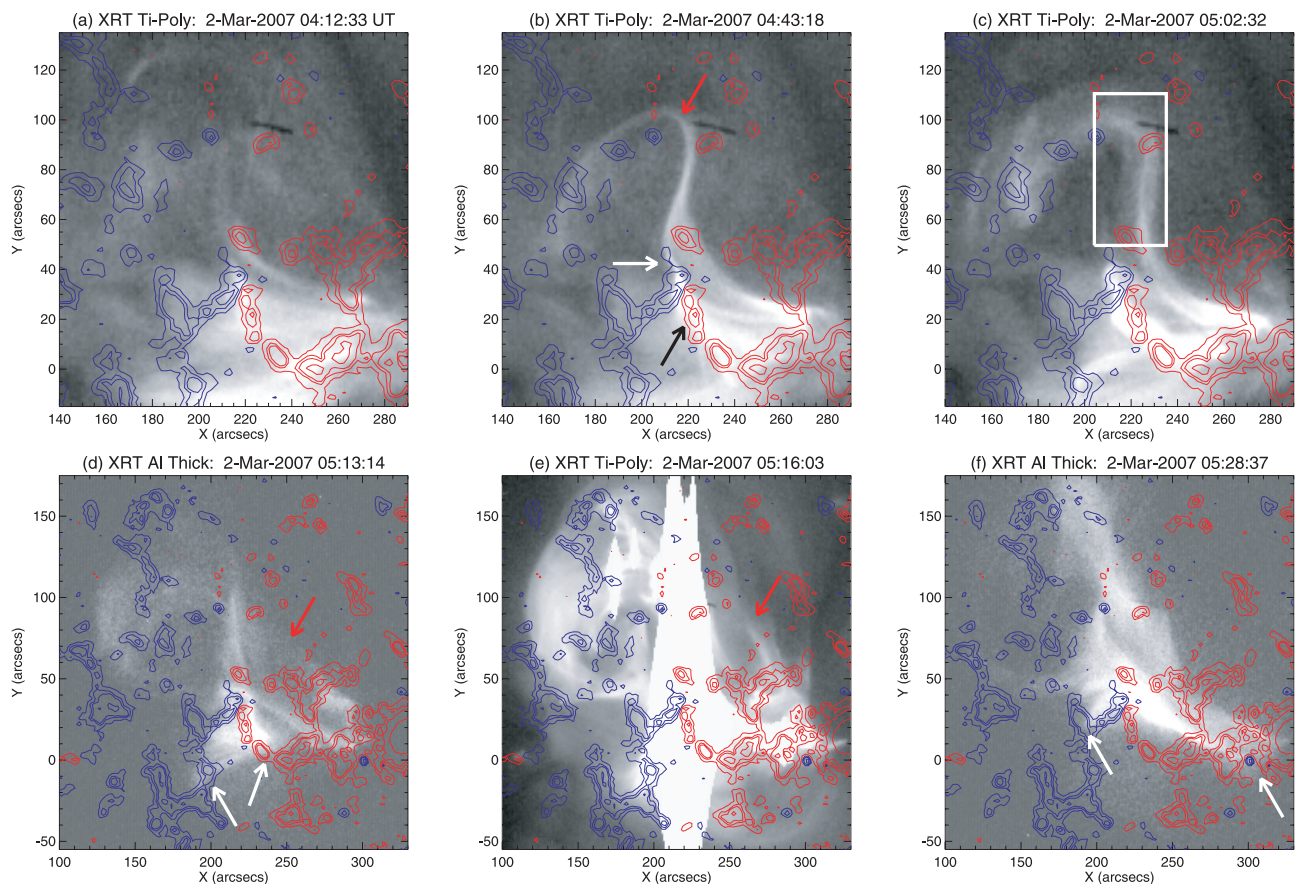


Fig. 2. Hinode XRT SXR images of the erupting region, on the same MDI magnetogram contours as in figure 1. Panels (a)–(c) are during the pre-eruption period, (d) and (e) are from about the time of the start of the eruption and the filament's fast rise, and (f) is near the time of the flare's peak intensity. In (b), the red arrow points to the north part of a sigmoid loop, and this corresponds to the EUV loop of figure 1b. The white and black arrows in (b) point out the roots of the lower reconnection product, and that loop appears bright in the XRT movie. In (d) and (e) the red arrows point to the middle part of the erupting sigmoid structure. White arrows in (d) and (f) point to the footpoints of bright loop arcades, which shift between the pre-eruption period of (d) and the time near the flare peak in (f). The bright streaking in (e) is due to saturation of the XRT CCD. In (c) the boxed region is used to generate the lightcurve in figure 3. Movie 2 is provided for the XRT images as on-line material* on the scale of panels (a)–(c).

episodes of reconnection in the middle of the sheared core field holding the filament.

At the base of the erupting location, the footpoints of the brightest SXR loops during the very early eruption phase (white arrows in figure 2d) are rooted in strong magnetic elements near the location where the sigmoid forms (white and black arrows in figure 2b), but later in the flare development, the situation changes so that the brightest loops have footpoints rooted farther away from the core (white arrows in figure 2f). This change may come about because of the attraction of the very strong field near the sunspot in the southwest [near coordinates (330'', 20'')] caused the feet of the reconnected field to jump to that strong field, or because the initial sigmoid eruption excited loops in a secondary episode that had pre-existing connections to the strong sunspot field. In the north of figure 2f there is additional strong SXR emission that may be due to field that may have opened (or partially opened) up due to complex secondary processes (such as ejection of a larger, overlying magnetic structure, e.g., Moore & Sterling 2007), although a comprehensive analysis of these features is beyond the scope of the present investigation.

3.3. Filament Motions

Figure 3 shows the trajectory, projected on the solar disk, of a portion of the filament as a function of time. It is undergoing a “slow-rise phase” from at least the time of the start of the TRACE observations, it undergoes a disturbance at about 04:45 UT, and has a “fast-rise phase” starting between 05:05 UT and 05:12 UT.

We chose to follow the filament along the figure 1a fiducial,

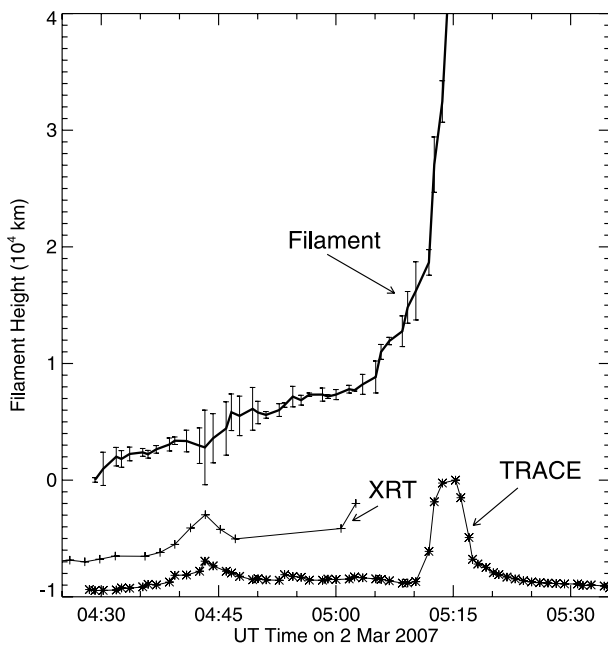


Fig. 3. Height as a function of time for a portion of the filament seen in TRACE images, along the fiducial of figure 1a. Error bars are 1σ uncertainties from three repeated measurements of the filament positions. Also shown are lightcurves of integrated intensities (with arbitrary vertical scaling) from TRACE and XRT from the boxed regions in figures 1b and 2c, respectively.

since along it we can track the pre-eruption motions relatively consistently; the orientation of the fiducial was selected to follow the approximate direction in which the filament is ejected out of the field of view. Actual motions of the filament, however, are complex, with different parts of the filament having different behavior (see movie 1). Thus, although the trajectory in figure 3 is indicative of the entire filament’s motion, detailed trajectories will differ for different parts of the filament. Our main emphasis is that there is a slow evolution (slow-rise phase) prior to the ejection (fast-rise phase). Also, it is difficult to sort out which of the filament’s motions are in the vertical direction. In fact, the filament undergoes a counter-clockwise twist between about 05:00 and 05:15 UT, and this is suggestive of a kink instability (similar to an event studied by Williams et al. 2005), as discussed further below. During the slow-rise phase, there is a burst in intensity in both the TRACE EUV images and in the XRT SXR images, in the lightcurves from, respectively, the location of the new EUV loop of figure 1b and the location where the sigmoid forms in figures 2a–2c; this burst disturbs the filament trajectory. Later, there is a bright flaring apparent in TRACE from 05:10 UT, while the XRT intensity is saturated due to flaring from 05:02:37 UT.

3.4. Magnetic Field Behavior

Both the west end (the source of the propagating emission) of the new loop of figure 1b and the point of formation of the sigmoid of figure 2b are at approximately the same location, viz. that indicated by the white and black arrows in figure 2b. From the MDI magnetograms in figures 1 and 2, this location is near a site of merging opposite-polarity magnetic elements along the neutral line of the pre-erupting filament. To gain clues to the source of these features, the likely ultimate source of the eruption, we investigate more closely the behavior of the magnetic field around this location with SOT.

Figure 4 shows SOT FG Stokes-V images around the erupting region. One can identify common features in figure 4a with the MDI magnetograms in figures 2d–2f, with the sunspot at the right edge near 20'' north. East of the spot are two partially-complete positive enhanced-network cells, and the furthest east of these flux cells butt up against part of an irregularly-shaped negative-polarity enhanced-network cell; the white box in figure 4a is centered on this colliding-positive-negative location. Again comparing with figure 1, we see that it is this location that contains the neutral line upon which the filament existed prior to eruption, and from where the eruption emanated.

Figures 4b–4d show the evolution over time of the field of the region of the white box in figure 4a. As mentioned in section 2, there is a time gap in these data, and it occurs between the images in figures 4b and 4c. A movie made from these SOT images (movie 3) however indicates that over this time gap the negative and positive regions flowed into each other. For example, both the large positive clump of field near (218'', 26'') and the negative clump near (205'', 40'') in figure 4b are not apparent in figure 4c; because of the overall flow pattern apparent in the movie, we assume that these clumps have each largely canceled with respective opposing polarities. This flow continues, and more flux has canceled by the time of figure 4d

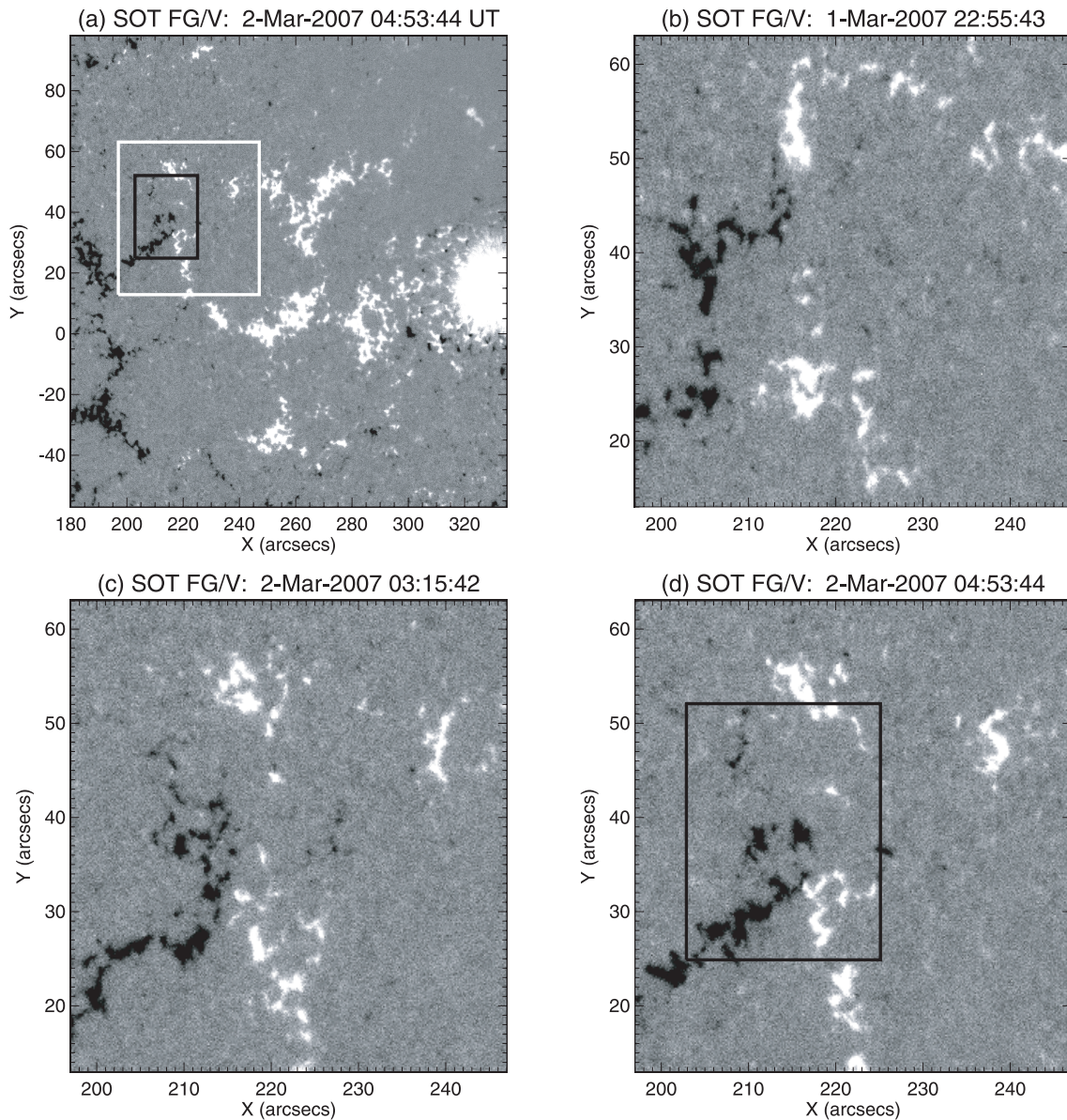


Fig. 4. SOT FG Stokes-V magnetograms of the erupting region. Comparing these with the MDI magnetogram and TRACE images of figure 1 shows the relation to the filament. Panel (a) is a context image showing a nearby sunspot, and panels (b)–(d) show a close-up of the neutral line under the erupting sigmoid, from the white box in (a), at different times. White and black show positive and negative polarities. These opposite polarities undergo flux cancellation over time, as calculations of the total unsigned polarity in the back box of (a) and (d) show (see text). Movie 3 is provided for the SOT images on the scale of panel (a) as on-line material.*

(which is identical to the time of figure 4a).

We would like to determine the amount of flux-change with time in the region around where the eruption appears to begin. We selected the black box in figure 4d (also shown in figure 4a) for this estimate. We did not, however, use the SOT data for this purpose, because as of the time of this writing those data are not yet calibrated. Instead, we measured the flux in the same location in the MDI images. We have three appropriate images, at 19:15 UT on 2007 March 1, and at 00:03 UT and 04:51 UT on 2007 March 2; in each case we have selected a box close to the black box of figure 4, but at each time we have adjusted the boundary slightly so that each box covers the same gross features. We found unsigned magnetic flux

values for these three times to be, respectively, 3.0×10^{19} Mx, 3.4×10^{19} Mx, and 1.0×10^{19} Mx. Thus, there is a substantial drop in the unsigned magnetic flux between 00 UT and the time of the eruption near 05 UT, and this is consistent with the flux cancellation shown by the SOT FG Stokes-V magnetograms. (Our MDI flux values do not include an adjustment factor obtained by Berger & Lites 2003, which would increase the stated values by about a factor of about 1.5.) From following some of the seemingly most rapid of the elements converging toward the neutral line between figures 4b and 4c, we deduced converging velocities of 0.45 ± 0.15 km s⁻¹, where the error is from uncertainty in identification of identical converging clumps of magnetic elements in the two frames.

4. Interpretation and Discussion

We can summarize our observations as follows. Over 20 min prior to the onset of strong SXR flare emission at 05:02 UT on 2007 March 2, an SXR sigmoid was growing via reconnection at the location of the white and black arrows in figure 2b, with these arrows showing the roots of the “lower reconnection product,” where the sigmoid is the “upper reconnection product.” Also during this pre-flare period there were slow motions of a filament visible in EUV. A new EUV loop appeared during the slow rise; to within our alignment accuracy, the EUV loop is a strand of the north portion of the XRT sigmoid. Thus both the north elbow of the sigmoid and EUV loop arch over the filament. Both the EUV loop and the site of the sigmoid formation undergo a burst in intensity, disturbing the filament’s slow rise, near 04:45 UT. Sterling and Moore (2005) and Sterling, Harra, and Moore (2007) have seen similar SXR intensity brightenings prior to the main flare that were related to the slow-rise phase of filaments, and this could be the flare precursor brightening discussed by Harrison (1986), which he suggested was related to CME onset. SOT and MDI data show that the location where the sigmoid forms and from where the EUV-loop emissions emanate are on a neutral line where opposite-polarity magnetic flux convergence had been occurring since at least 22 UT on March 1.

Figure 5 shows our interpretation of these observations. The green and magenta field lines are poised to reconnect, forming the low-lying black loop and an out-moving sigmoid loop. There would be other loops similar to the green and

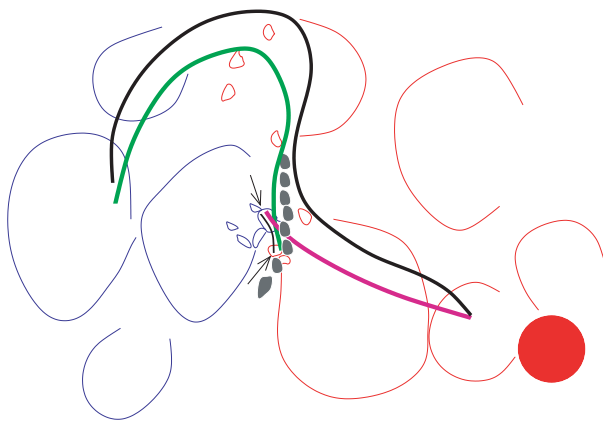


Fig. 5. Schematic interpretation of the eruption of figures 1–4. Red and blue contours roughly correspond to the magnetic pattern in the MDI (figures 1 and 2) and SOT FG Stokes-V (figure 4) magnetograms, with the red circle in the lower right representing the sunspot, and the broken shaded feature represents the filament along the neutral line of the black box of figure 4. The green field curve represents the loop seen in EUV (figure 1b), and in the north part of the sigmoid of figure 2. The magenta curve represents a field line extending from the region around the sunspot in figures 2d–2f. Magnetic reconnection between the field of the green and magenta structures results in two reconnection products: the sigmoid of figure 2, and smaller loops that straddle the neutral line and which have footpoints indicated by the two arrows, and these correspond to the white and black arrows in figure 2d; both of these reconnection products are drawn as black lines in the schematic.

magenta loops that would subsequently reconnect, although clumps of magnetic field in the photosphere would tend to make the reconnection episodic; this would account for the fainter-illumination sigmoid fields that we see in the XRT images prior to production of the bright sigmoid of figures 2b and c. Reconnection of these fields reduces field restraining the filament field, and results in the slow rise of the filament; Moore and Roumeliotis (1992) discussed the slow start to eruptions by such processes, which they called “slowly driven tether cutting.” Sterling, Harra, and Moore (2007) present a slightly different example where “tether weakening” reconnection appears to be occurring. In both cases, we propose that each reconnection episode results in a further rise of the filament.

Key to the reconnections at the crossing point of the figure 5 green and magenta field lines, is the converging of the photospheric magnetic field as revealed by the SOT FG Stokes-V data. Cancellation of this flux at the neutral line leads to reconnection at the green–magenta field crossing point (which is near location of the white arrow in figure 2b), producing the short lower reconnection loop and the rising filament-holding SXR sigmoid, the activation and slow rise of the filament, and eventually to disruption of the whole field system resulting in the fast filament rise in the violent eruption.

From the fluxes derived from the MDI data in the previous section, we can make an estimate of the strength of the field above the noise level (which we take as 10 G) in the region of the black box in figures 4a and d, and we derived this strength, B , to be about 40 G. (The 1.5 factor of Berger & Lites 2003 would make this 60 G.) Thus the fields are not very strong. Moreover, we measure that the entire erupting and flaring region, which we estimate to span $150''$ – $300''$ in x and $0''$ – $150''$ in y (see e.g., figure 2, however this ignores possible secondary eruptions covering a larger area), to have flux $\sim 5 \times 10^{20}$ Mx, and so a flux change of $\sim 5\%$ over the last 5 hours prior to eruption is enough to begin the release of energy contained in the pre-existing sheared field by some mechanism, such as an instability, leading to the eruption. van Ballegooyen and Martens (1989) suggested that long-term flux cancellation can result in filament-supporting flux-tube geometries, and to the eventual destabilization and eruption of the filament; this could be what is occurring here.

The erupting sigmoid loop we see in figure 2 is similar to the type described by Rust and Kumar (1996) and Pevtsov, Canfield, and Zirin (1996), where the sigmoid loop is made by the reconnection of the crossed arms of the elbows in the onset of eruption, in contrast to the longer-lasting sigmoid-shaped active regions discussed by, e.g., Canfield, Hudson, and McKenzie (1999) and Sterling et al. (2000). Both types, however, are a consequence of the sheared nature of the magnetic field in erupting regions and many active regions. Moore et al. (2001) also saw a developing sigmoid of the type we observed here (see their figure 5).

Rust and Kumar (1996) also discussed the kink-mode instability in the context of eruptions. Our filament underwent writhing near the onset of the fast-rise phase, and so a combination of tether-weakening reconnection, along with tether-cutting reconnection and the kink instability could be the release mechanism for the fast-rise phase of the eruption; this

is similar to the conclusion reached by Williams et al. (2005) for a filament eruption they observed.

We thank the anonymous referee for useful comments. A.C.S. and R.L.M. were supported by funding from NASA's Office of Space Science through the Solar Physics Supporting Research and Technology Program and the Sun–Earth Connection Guest Investigator Program. Hinode is a Japanese mission developed and launched by ISAS/JAXA, collaborating with NAOJ as a domestic partner, NASA and STFC (UK

as international partners. Scientific operation of the Hinode mission is conducted by the Hinode science team organized at ISAS/JAXA. This team mainly consists of scientists from institutes in the partner countries. Support for the post-launch operation is provided by JAXA and NAOJ (Japan), STFC (U.K.), NASA, ESA, and NSC (Norway). We also acknowledge the invaluable contribution made to the Hinode project by our colleague and friend, Dr. Takeo Kosugi, who sadly passed away shortly after Hinode's launch.

References

- Alexander, D., Metcalf, T. R., & Nitta, N. V. 2002, *Geophys. Res.* 29, L1403
- Berger, T. E., & Lites, B. W. 2003, *Sol. Phys.*, 213, 213
- Canfield, R. C., Hudson, H. S., & McKenzie, D. E. 1999, *Geophys. Res.*, 26, L627
- Culhane, J. L., et al. 2007, *Sol. Phys.*, 243, 19
- Feynman, J., & Ruzmaikin, A. 2004, *Sol. Phys.*, 219, 301
- Golub, L., et al. 2007, *Sol. Phys.*, 243, 63
- Handy, B. N., Bruner, M. E., Tarbell, T. D., Title, A. M., Wolfson, C. J., Laforge, M. J., & Oliver, J. J. 1998, *Sol. Phys.*, 183, 29
- Harrison, R. A. 1986, *A&A*, 162, 283
- Kahler, S. W., Moore, R. L., Kane, S. R., & Zirin, H. 1988, *ApJ*, 328, 824
- Kosugi, T., et al. 2007, *Sol. Phys.*, 243, 3
- Moore, R. L., & Roumeliotis, G. 1992, in *Eruptive Solar Flares*, ed. Z. Svestka, B. V. Jackson, & M. E. Machado (Berlin: Springer), 69
- Moore, R. L., & Sterling, A. C. 2007, *ApJ*, 661, 543
- Moore, R. L., Sterling, A. C., Hudson, H. S., & Lemen, J. R. 2001, *ApJ*, 552, 833
- Pevtsov, A. A., Canfield, R. C., & Zirin, H. 1996, *ApJ*, 473, 533
- Roy, J.-R., & Tang, F. 1975, *Sol. Phys.*, 42, 425
- Rust, D. M. 1976, *Sol. Phys.*, 47, 21
- Rust, D. M., & Kumar, A. 1996, *ApJ*, 464, L199
- Scherrer, P. H., et al. 1995, *Sol. Phys.*, 162, 129
- Sterling, A. C., Harra, L. K., & Moore, R. L. 2007, *ApJ* in press
- Sterling, A. C., Hudson, H. S., Thompson, B. J., & Zarro, D. M. 2000, *ApJ*, 532, 628
- Sterling, A. C., & Moore, R. L. 2004, *ApJ*, 602, 1024
- Sterling, A. C., & Moore, R. L. 2005, *ApJ*, 630, 1148
- Tandberg-Hanssen, E., Martin, S. F., & Hansen, R. T. 1980, *Sol. Phys.*, 65, 357
- Tsuneta, S., et al. 2007, *Sol. Phys.* submitted
- van Ballegoijen, A. A., & Martens, P. C. H. 1989, *ApJ*, 343, 971
- Williams, D. R., Török, T., Démoulin, P., van Driel-Gesztelyi, L., & Kliem, B. 2005, *ApJ*, 628, L163